Validation and verification of FE models of piezo based SHM systems

Etienne Balmès, Mikhail Guskov, Jean-Philippe Bianchi

Validation and verification of FE models of piezo based SHM systems

E. Balmes [2,1]**, M. Guskov**[2]**, J.P. Bianchi**[1]
[1]SDTools
44 rue Vergniaud, 75013, Paris, France
e-mail: **balmes@sdtools.com**

[2]Arts et Metiers ParisTech, PIMM
151 Boulevard de l'Hôpital, 75013, Paris, France

Abstract
The idea of generating and sensing Lamb waves through piezoelectric sensor/actuator configurations is common for Structural Health Monitoring (SHM) applications. Methods using time of flight analysis require the prediction of the first incoming waves. Computations on small periodic patterns are shown to be usable to determine which waves will actually be relevant. For the considered applications, these are the first membrane waves propagating at fairly high speeds. Parametric FEM computations are then used to analyze important parameters (mesh size, time step, damping) and it is shown that accurate predictions can be obtained in a few CPU minutes.

1 Introduction

The idea of generating and sensing Lamb waves through piezoelectric sensor/actuator configurations has been considered by several authors for Structural Health Monitoring (SHM) applications. In the framework of the CORAC/Coralie project [1, 2, 3, 4], components of aircraft nacelles composed of standard monolithic multi-layer laminates and honeycomb assemblies were considered and will be used here. Figure 1 illustrates a network of piezoelectric patches which are used to generate and sense pulses in the 100-1000 kHz range.

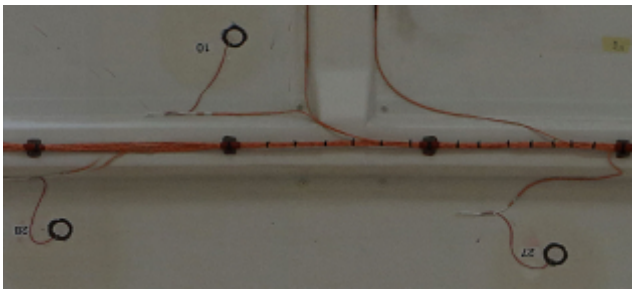

Figure 1: Aircraft nacelle equipped with piezo-electric patches.

Figure 2 illustrates the propagation of a wave associated with such pulses in the rectangular plate configuration used for test/analysis correlation. On the left, the lower left piezo is used as a source and interaction with the damage (small circle marked as damage) is not clearly visible. On the right, the figure illustrates the difference between the responses of the healthy and damaged structures. The damage then clearly acts as a wave

source, which gives a direct understanding of how SHM methods may work by comparing healthy/damaged signals.

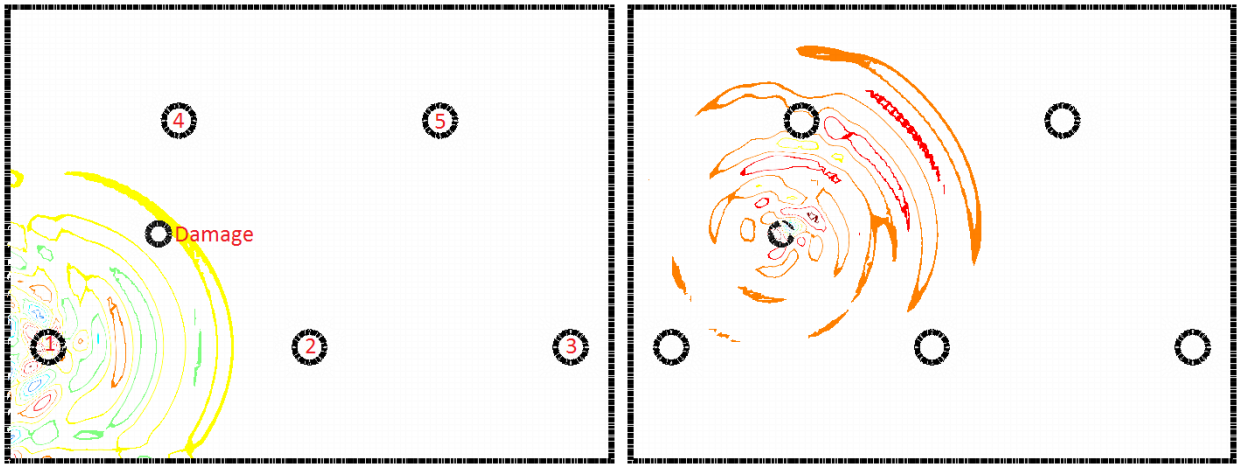

Figure 2: Left : wave front generated by a CosHan excitation centered around 200 kHz. Right : difference between wave fronts of healthy and damaged configurations.

The main steps of SHM process are detection, localization, assessment of damages and prediction of the structure state [5]. Investigations on large sets of configurations, in terms of sensor setup, material configurations, environment parameters such as temperature, damage location and severity, would enable to compensate for environment conditions variations [3], enrich the subsequent statistical learning and to maturate the SHM procedures [4]. While experimental tests can be used to demonstrate the validity of processes in certain configurations, their number is fundamentally limited. In this context, the ability to have predictive models is particularly important and will be discussed here.

The focus in this work will be put on simulations for damage localization techniques based on time of flight analyses. These approaches use the time of arrival on sensors of the first incoming wave packet due to a voltage pulse applied to a piezo patch [2]. These methods benefit form the direct wave travel, thus allowing minimal simulation times excluding the influence of boundary conditions and narrowing the analysis to the time of direct propagation of the first wave packet. Note that other SHM stages, such as detection or assessment could involve longer term vibration patterns. For instance, damage indicators based on post-arrival parts of measured signals have been used in statistical learning methods for detection.

The development of FEM models for SHM applications has been discussed in many papers and books [6, 7, 8, 9]. However, most of these numerical investigations represent either methodological research on rather simple structures, such as beams [10], or detailed phenomenological analysis on a refined FE model, featuring complex wave behaviors in a more detailed framework (wave generation and propagation [11], or wave-damage interaction [12]). Using the finite element models of structures equipped with piezoelectric elements implemented in the SDT [13], the specific contribution of this paper is thus a discussion of steps involved in the evaluation models needed to properly simulate healthy and damaged configurations.

For the case of SHM indicators based on the analysis of the incoming waves, it is important to understand which waves will propagate fastest and will be actually observed. Section 2 will use periodic computations to estimate the propagating waves in the frequency range of interest (pulses centered around frequencies up to 200 kHz) for both the straightforward laminate and a more difficult honeycomb configuration.

The second difficulty addressed in section 3 is to verify and validate models. Needs in terms of mesh refinement, time step and damping modeling are then discussed. Test/analysis correlation shows the validity of proposed models in both laminate (shell and piezo-shell) and honeycomb (shell/volume/shell and piezo shell) configurations and illustrate that the numerical cost of such transient computations, as implemented in SDT, is fairly low.

2 Estimating Lamb waves in complex configurations

The first issue when designing a Lamb wave based SHM procedure is to establish the waves that will be excited and measured at piezo-elements.

In a basic laminated plate configuration, semi-analytical approaches exist [14, 15], but it is interesting to note that periodic computations can be used to analyze all possible waves at a fairly low cost, while enabling a much higher fidelity of structural behavior representation. This can be of particular interest in the case of honeycomb core sandwich panels where the detailed cell model would enable representation of cell wall modes.

2.1 Periodic solutions in the spatial domain

A key property of periodic systems, see for example [16], is that for excitations at a given wavelength, described as a field on the nominal cell $U(x_0, \kappa_{cx})$ associated with a single wavenumber κ_{cx}, the only response occurs at the same wavelength κ_{cx} provided that the geometry and model properties are strictly periodic. A large FEM problem with repeated slices can thus be decomposed in a series of independent problems for single wavenumbers, which correspond to periodic solutions.

For a solution with a single wavenumber κ_{cx}, the field is simply equal to

$$u(x_0 + n\Delta x) = \Re(U(x_0, \kappa_{cx})e^{i\kappa_{cx}n}), \tag{1}$$

which will be used to compute the periodic solutions. In the case of structures represented as FE models, the continuous displacement in the nominal cell $u(x_0)$ is discretized and replaced by a vector $\{q\}$ of Degrees Of Freedom (DOF) values.

To ensure the displacement continuity between adjacent periodic cells, a continuity condition must be introduced. The displacement on the left boundary of one cell has to be equal to the one of the preceding cell right edge, thus $\{q_{left}(n\Delta x)\} = \{q_{right}((n-1)\Delta x)\}$. Following the definition given in the previous section, $\{q_n\}$ represents all the displacements at the DOF of the cell number n. For each cell, the observation matrices $[c_l]$ and $[c_r]$ can then be defined to extract from the whole DOF set the ones corresponding to respectively left and right boundaries. These matrices are the same for all cells if the domain is meshed regularly.

For a periodic response associated with a single wavenumber, taking into account Eq. (1), the continuity condition can be written as $[c_l]\{Q(\kappa_{cx}, \omega)\} = [c_r]\{Q(\kappa_{cx}, \omega)\}e^{-2i\kappa_{cx}}$ which, differentiating real and imaginary parts, leads to

$$[C(\kappa_{cx})] \begin{Bmatrix} \mathrm{Re}(Q(\kappa_{cx}, \omega)) \\ \mathrm{Im}(Q(\kappa_{cx}, \omega)) \end{Bmatrix} = 0, \tag{2}$$

with

$$[C(\kappa_{cx})] = \begin{bmatrix} [c_l] - \cos(\kappa_{cx})[c_r] & -\sin(\kappa_{cx})[c_r] \\ \sin(\kappa_{cx})[c_r] & [c_l] - \cos(\kappa_{cx})[c_r] \end{bmatrix}.$$

For an external force $\{f\}$ applied to the system, s being the Laplace variable, the first step is to compute the Floquet (spatial Fourier) transform of the load $F(\kappa_{cx}, s)$. Then the equations of motion, which are known to be decoupled for each wavenumber, take the frequency domain form

$$[Z(\omega)]\{Q(\kappa_{cx}, \omega)\} = \{F(\kappa_{cx}, \omega)\}, \tag{3}$$

where $Z(\omega) = -M\omega^2 + K$ is the dynamic stiffness matrix. This matrix contains mass M as well as stiffness and damping in the matrix K. The matrix K can take into account hysteretic damping (constant imaginary part of K) or viscoelastic contributions (frequency and temperature dependent $K(\omega)$), see [17].

Material	Monolithic	Skin 1	Skin 2
E_{11}, GPa	69	66	61
E_{22}, GPa	69	66	61
E_{33}, GPa	8.1	8.1	8.1
G_{12}, GPa	4.8	5.2	5.2
G_{13}, GPa	4.8	5.2	5.2
G_{23}, GPa	4.8	5.2	5.2
ν_{21}	0.03	0.02	0.02
h, mm	0.28	0.28	0.3
ρ, kg/m^3	1554	1554	1583

Table 1: Nominal mechanical properties of orthotropic laminate composite material layer

Since the frequency response can be complex in the spatial domain, it is necessary to distinguish real and imaginary parts of the spatial transform. The equations actually solved are thus

$$\begin{bmatrix} Z(\omega) & 0 \\ 0 & Z(\omega) \end{bmatrix} \begin{Bmatrix} \text{Re}(\{Q(\kappa_{cx},\omega)\}) \\ \text{Im}(\{Q(\kappa_{cx},\omega)\}) \end{Bmatrix} = \begin{Bmatrix} \text{Re}(F(\kappa_{cx},\omega)) \\ \text{Im}(F(\kappa_{cx},\omega)) \end{Bmatrix}, \tag{4}$$

with (2) verified.

Solution of a linear system Eq. (4) with constraint (2) is here obtained by elimination. The continuity condition is thus taken into account by first seeking a basis T of $\ker([C(\kappa_{cx})])$. Then this basis is used to find the solution of the constrained problem

$$\left([T]^T [Z(\kappa_{cx},\omega)] [T]\right) \{Q(\kappa_{cx},\omega)\} = [T]^T \{F(\kappa_{cx},\omega)\}. \tag{5}$$

Solving directly this problem can be fairly long as it requires inversion of the constrained dynamic stiffness $T^T Z(\omega) T$ at each desired frequency. Modal synthesis methods which combine modes and static corrections for loads, and possibly viscoelastic loads [18], are thus preferred here.

2.2 Laminated composite

In the simple case of a 4 ply composite (each ply is a carbon textile-reinforced epoxy, see column "Monolithic" in Table 1), the representative volume mesh can be a simple column as shown in figure 3 left. The dispersion curve can be computed as shown in figure 3 center. The frequency range of interest is below 500 kHz. In this range the only existing waves are the first 3. Based on the dispersion curves, the group velocity can be estimated using

$$v_g = \frac{\partial \omega}{\partial k} \tag{6}$$

For the 3 waves propagating below 500 kHz, the group velocities associated with a volume and shell model are overlaid in 3 right. The first mode, in blue, corresponds to bending. Its group velocity increases rapidly at low frequencies then tends to be fairly constant. The second mode is an in-plane shear mode with a constant velocity near 3510 m/s. The third mode is an in-plane traction/compression with a velocity close to 5930 m/s. The nature of the mode is readily seen by animating the mode shape for a relatively short wavelength. The figure also illustrates that the group velocities of the in plane modes are nearly identical for volume and laminated shell models.

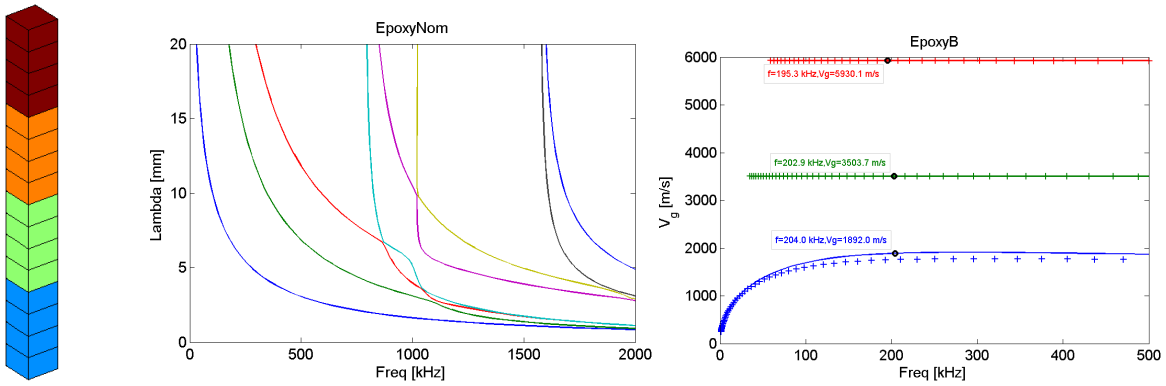

Figure 3: Left: representative volume. Center : dispersion curve for nominal laminate. Right : estimated group velocities

For easy use of time of flight strategies [2], it is necessary to limit distortion of the waveform during propagation. For the bending waves, group velocity increases fairly rapidly up to 100 kHz, it is thus necessary to use higher frequencies for proper application of the methodology.

Since the material is anisotropic and due to the low Poisson's ratio not transversely isotropic, one expect that the in plane stiffness of a ply should be lower at 45^o.

By computing waves propagating at various angles one can estimate modal frequencies and group velocities as a function of angle as shown in figure 4 left. The layup of 0,45,45,0 is meant to generate a nearly isotropic material. This is well found for in-plane modes where each ply has the same influence, while for the bending mode, the top and bottom plies have more influence and an angular dependence is clearly visible in figure 4 right.

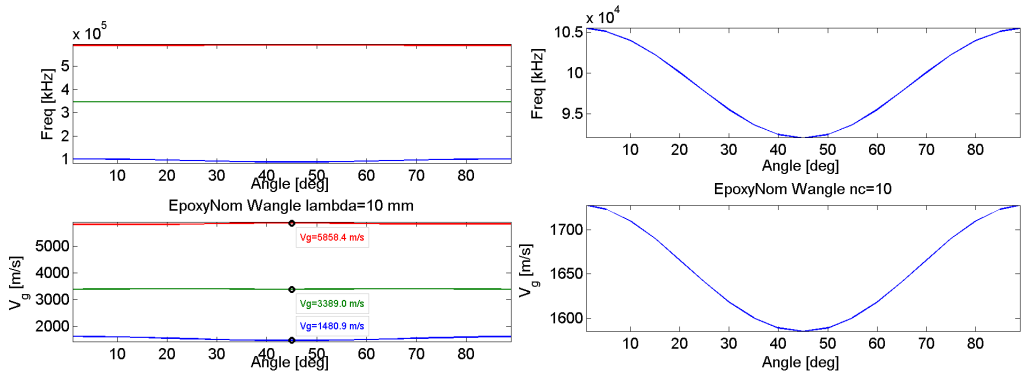

Figure 4: Influence of orientation on group velocity. Left : volume model 3 modes. Right : zoom on bending mode

2.3 Honeycomb

Now considering the case of a sandwich panel, composed by two monolithic skin sheets (see table 1) and honeycomb core (made of 30 mm wide, 0.1 mm thick aluminum foil, with 10 mm cells), one is interested in understanding propagation of in-plane "membrane modes" in the skins (often referred to as the S0 waves in the Lamb wave literature). The base cell shown in Figure 6 is modeled using 556 quadratic volume elements for 11000 DOF including 1350 interface nodes making the cost of WFE [19, 20] approaches significant. To focus on in-plane waves a symmetric in-plane loading of the top and bottom skins is applied and the transfer function to the mean in-plane response on the two skins is shown in Figure 5. This transfer function is shown in the frequency/wavenumber domain and is thus called a 2D-DSFT transfer (discrete space Fourier transform [21]).

The black lines on the plot show the dispersion diagram. A high number of propagating waves clearly exist. Bending, indicated as point (a) (with the corresponding modeshape in figure 6), occurs first but is not excited by the considered load and thus does not lead to peak in the 2D-DSFT transfer. A large number of wall bending modes, point (b) for example, occur at relatively low frequencies due to the small thickness of the honeycomb walls. These modes are propagating slowly since the $\partial\omega/\partial k$ slope is small.

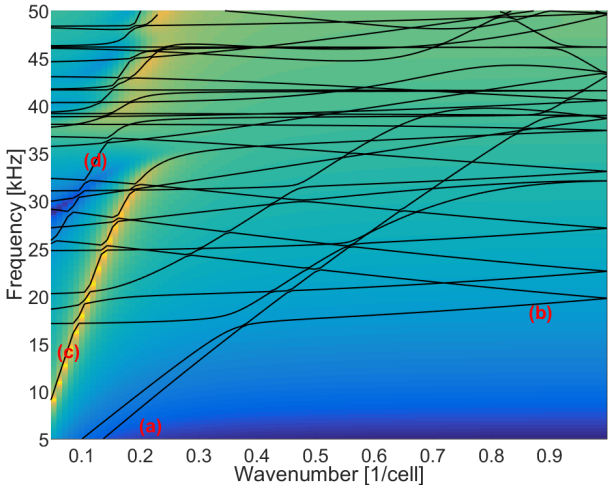

Figure 5: Transfer associated with an in plane load in the frequency-wavenumber domain.

The in-plane wave of interest is indicated by point (c) and its evolution with frequency is clearly indicated by the peak of the transfer function. The second mode propagating with the same group velocity is the anti-symmetric in-plane mode (d). An interesting feature of this response is the existence of a band-gap between 33 and 40 kHz.This gap is associated with distributed resonating substructures, which here correspond to the honeycomb wall bending.

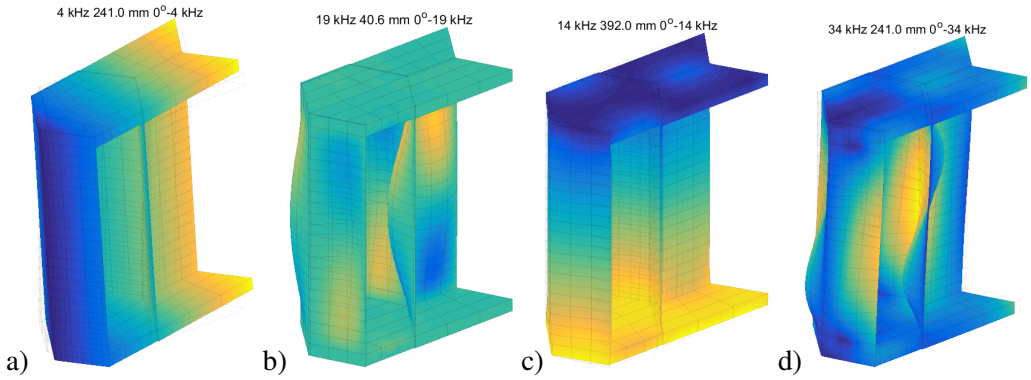

Figure 6: Sample wave shapes. a) bending mode, b) first wall bending, c) symmetric in-plane compression, d) anti-symmetric in-plane compression

3 Validation and verification of a FEM model

3.1 Modeling in the epoxy configuration

Once the nature and characteristic group velocities of propagating waves of interest known, it becomes possible to start making choices for a full FEM model prediction. The predictions of interest are illustrated

in figure 7. An electric pulse is generated in piezo 1 (see location in figure 2), the incoming waves are then sensed on electrodes of other piezo patches. Piezos 2 and 4 have are distant from 173 mm, 5 from 300 mm and 3 from 346 mm. Time of flight estimation, based on the Hilbert transform, is discussed in [3].

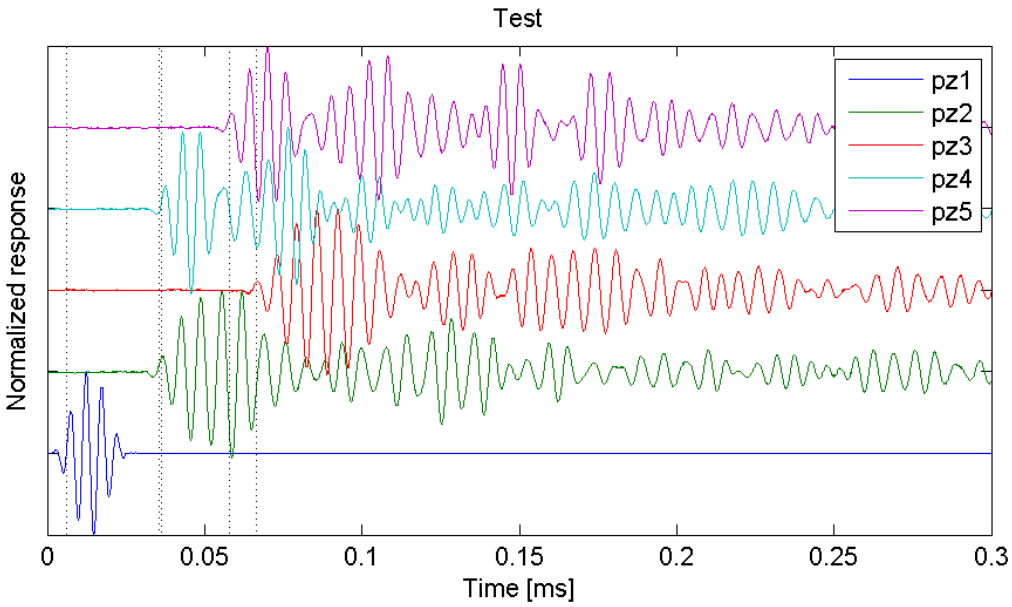

Figure 7: Normalized test responses to excitation on piezo 1.

Shell models are well suited for membrane, bending and shear representation. For the laminate of section 2.2, shells can thus be used up to 800 kHz. For the honeycomb of section 2.3, the waves of interest and in-plane waves and the classical shell/volume/shell [8] representation of honeycomb panels is sufficient provided that bandgaps do not interact with the response.

Given the continuous model, further FEM parameter choices are linked to mesh size in uniform areas, mesh refinement around gradient areas (piezo-patches and damage visible in figure 2), time step, damping. To allow study of such parameters, a parametric model was generated using SDT capabilities. Steps of this parametric study are

- automated meshing from a configuration listing materials, positions and diameters of piezo-patches, names in the patch catalog, position and nature of damage, honeycomb details, ...
- transient simulation using an implicit Newmark scheme using voltage input.
- post-processing including extraction of electric responses, generation of specific FEM views or movies.

Computation of target mesh size is classically based on understanding of wave-lengths. For the laminate case, wave velocities at 5930 m/s and a wave-front period of $5\mu s = (200kHz)^{-1}$ that should be divided in at least 6 to describe a period, leads to a theoretical target mesh length close to $5mm$. To verify the convergence a study was performed with characteristic mesh lengths at 3, 5 and 8 mm. Figure8 illustrates that the convergence depends on the feature of interest. For the first burst, the amplitude and arrival time errors are quite small. The amplitude is however problematic for $Lc = 8mm$ and times in the 0.1 to 0.15 ms range.

The automated meshing procedure leads to mesh sizes of 338,974 DOF, 126,538 DOF, 51,286 DOF. In terms of CPU, the runs take 15 mn, 6 mn and 2 mn for a simulation of 1334 time steps at $dt = 3^{e-7}s$. Such times are quite compatible with parametric studies on excitation, damage location, ... that are of typical interest in SHM applications.

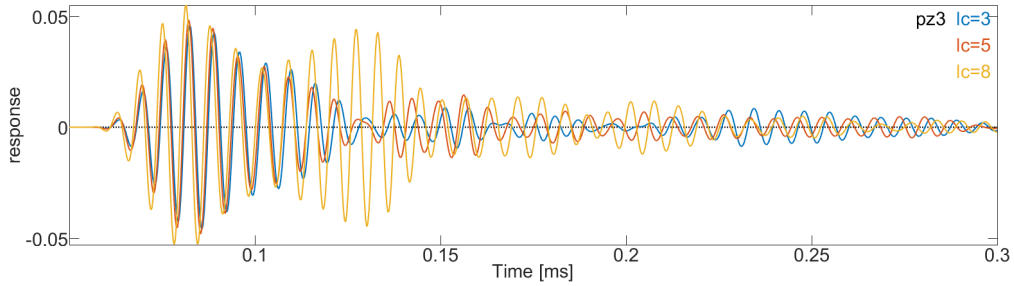

Figure 8: Mesh refinement study. Epoxy laminate, response at piezo 3.

The second convergence study is performed on time step shown in figure 9. With $dt = 5e-7s$, amplitude and phase errors are notable, leading to phase opposition of the wave front at times around $0.12ms$. With $dt = 2.5e-7s$, results are not perfect but quite relevant. Link to amplitude and phase errors associated with the implicit Newmark scheme used here can be found in Ref. [22].

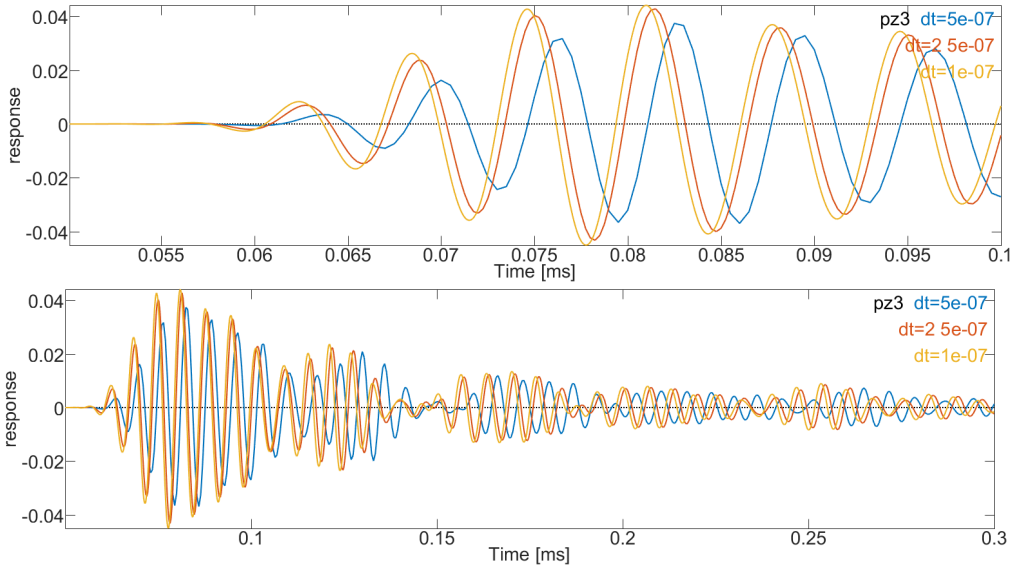

Figure 9: Healthy epoxy. Actuator: Pz1. Convergence with time step.

Another critical parameter is damping. Realistic damping models consider viscoelastic or hysteretic damping, but are hard to implement in the time domain. The usual assumption is thus to use Rayleigh damping despite its shortcomings. Nominal damping was chosen at $C = \beta K = 2.5e-8K$, which corresponds to a modal damping ratio of

$$\zeta = \frac{\beta\omega}{2} = 1.57\% \text{ at 200 kHz.}$$

Figure 10 illustrates that damping affects amplitude notably with a small impact on the signal shape visible in the bottom graph.

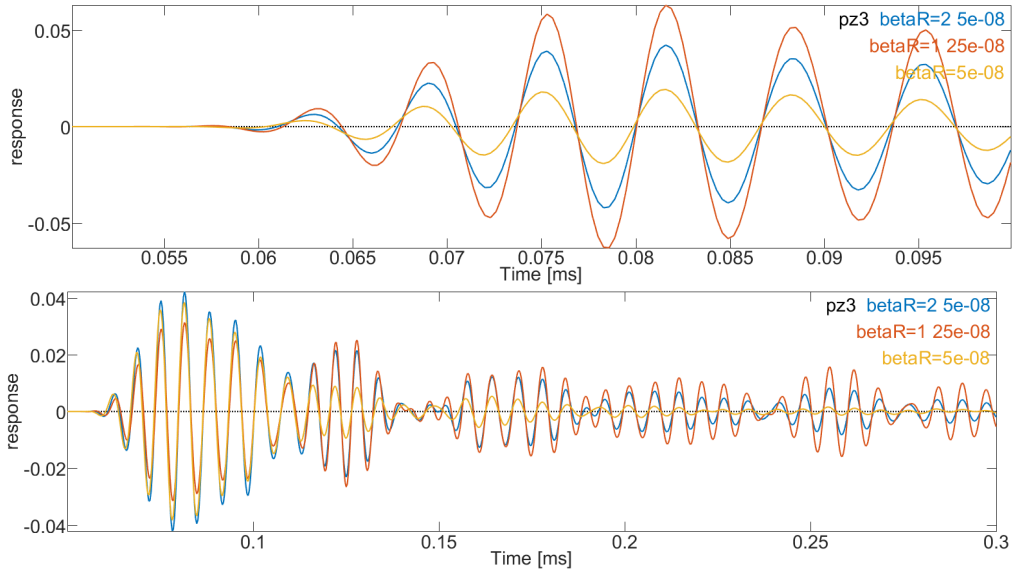

Figure 10: Influence of Rayleigh damping. Epoxy. Top: zoom in signal arrival. Bottom : signals scaled by the presence of β factor.

Finally, figure 11 addresses the impact of the plate modulus, which can vary with temperature in particular. The figure clearly shows the direct impact of modulus on the time of flight. It is thus possible to identify modulus properties from such predictions. In the current laminate case, velocity estimates are quasi-isotropic with respect to directions as expected and are in the 5124 to 5473 m/s range which is relatively close from the estimate with nominal material parameters.

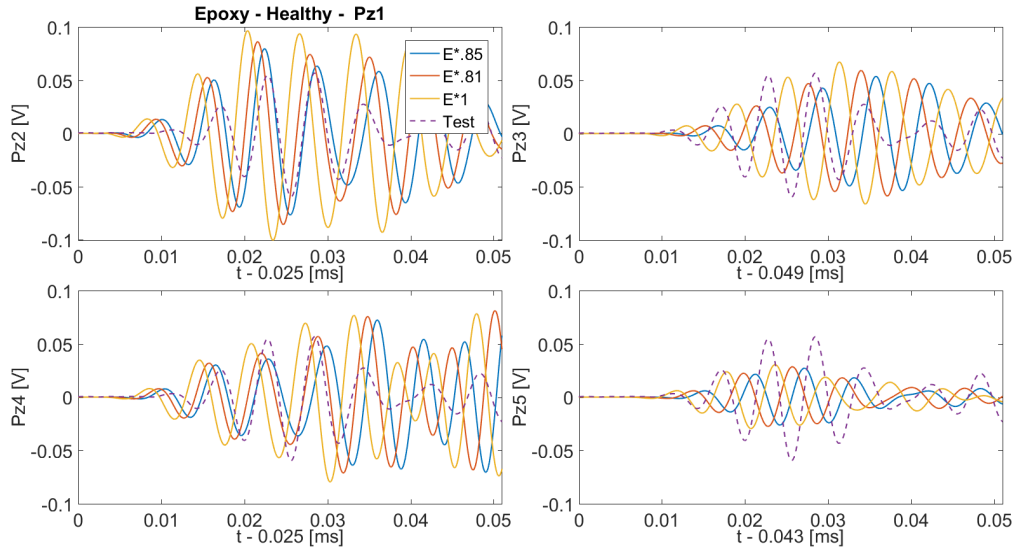

Figure 11: Influence of Young's modulus on wave fronts at different sensors.

3.2 Honeycomb

Now considering the honeycomb, a transient simulation for excitation at piezo 1 was performed with $Lc = 4mm$. The shell/volume/shell model has 102,784 DOF and the implicit transient simulation took 4 mn (or 180 ms per time step) which remains quite acceptable for parametric studies. Figure 12 left, showing a color to proportional to in-plane displacement, illustrates that in-plane membrane waves propagate fastest on the

skins as was expected from section 2.3. The excitation occurs on the top face and the figure thus illustrates that while excitation is indeed transmitter to the bottom layer, there is a phase difference due to transmission through the honeycomb core.

In the test, observed group velocities are again fairly isotropic and correspond to the experimentally observed values in the 4518 to 4654 m/s range which is compatible with the level of uncertainty on material properties.

The plots on the right, showing a color proportional to normal displacement, illustrate the propagation of the slower skin bending waves. The propagation shows some anisotropy as was expected since the ply layup is only isotropic for in plane behavior. The relatively irregular wave front illustrates the fact that the mesh size is actually not sufficient for the shorter wavelength bending waves.

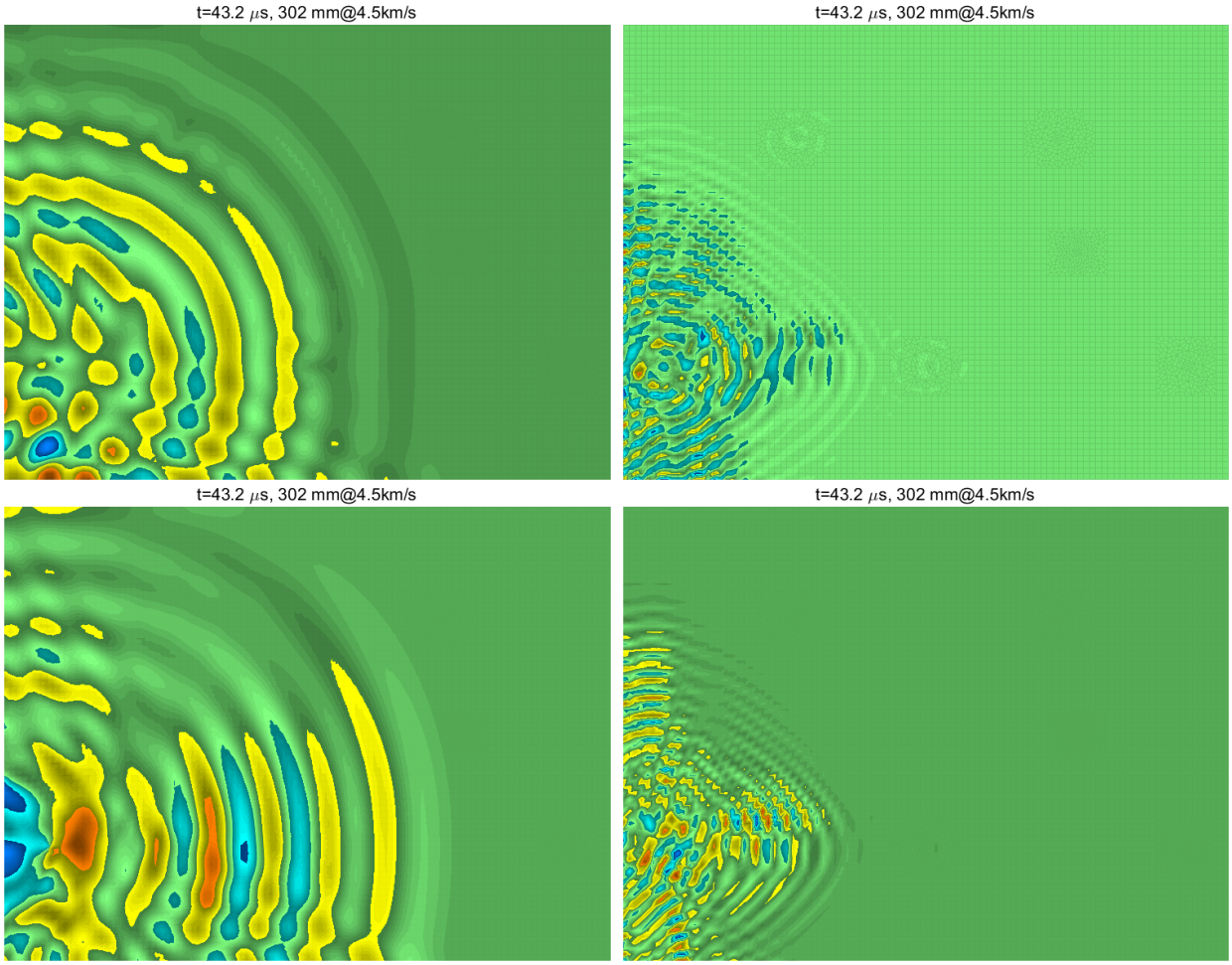

Figure 12: Shell volume shell model with vertical displacement as color. Left/right : in/out of plane motion. Top/bottom : piezo/opposite face

4 Conclusion

SHM applications using time of flight analysis require the prediction of the first incoming waves. Computations on small periodic patterns were shown to be usable to determine which waves will actually be relevant. For the considered applications, these were the first membrane waves propagating at fairly high speeds. The usual SHM reference to Lamb waves is thus somewhat fancy for a configuration of plane stress motion for both the classical laminate and honeycomb configurations.

Once the modeling objectives established the parametric capabilities of SDT were used to perform a number of sensitivity analyzes showing that accurate predictions can be obtained in a few single core CPU minutes. The main parameters driving numerical cost are mesh refinement, which is not too problematic since in-plane waves are of interest, and duration of signal of interest, which is quite accessible for time of flight studies. Damping remains a parameter that is not properly modeled but, for the relatively narrow band signals considered, adjustment of a Rayleigh coefficient by correlation with test amplitudes seems relevant. Test analysis correlation is then fairly good and quite sufficient for use of models as proofing and maturation tools for SHM detection or localization algorithms.

References

[1] C. Fendzi, J. Morel, M. Rebillat, M. Guskov, N. Mechbal, and G. Coffignal, "Optimal Sensors Placement to Enhance Damage Detection in Composite Plates," *7th European Workshop on Structural Health Monitoring*, July 2014.

[2] C. Fendzi, N. Mechbal, M. Rebillat, M. Guskov, and G. Coffignal, "A general Bayesian framework for ellipse-based and hyperbola-based damage localization in anisotropic composite plates," *Journal of Intelligent Material Systems and Structures*, vol. 27, no. 3, pp. 350–374, 2016.

[3] C. Fendzi, M. RŽbillat, N. Mechbal, M. Guskov, and G. Coffignal, "A data-driven temperature compensation approach for Structural Health Monitoring using Lamb waves," *Structural Health Monitoring*, p. 1475921716650997, 2016.

[4] O. Hmad, C. Fendzi, N. Mechbal, and M. Rebillat, "Verification and Validation of Structural Health Monitoring Algorithms: A Maturation Procedure," *IFAC-PapersOnLine*, vol. 48, pp. 952–957, Sept. 2015.

[5] K. Worden and G. Manson, "The application of machine learning to structural health monitoring," *Philosophical Transactions of the Royal Society of London A: Mathematical, Physical and Engineering Sciences*, vol. 365, no. 1851, pp. 515–537, 2007.

[6] Z. Su and L. Ye, *Identification of damage using Lamb waves: from fundamentals to applications*, vol. 48. Springer Science & Business Media, 2009.

[7] S. Gopalakrishnan, M. Ruzzene, and S. V. Hanagud, *Computational techniques for structural health monitoring*. Springer series in reliability engineering, London: Springer, 2011.

[8] E. Balmes and C. Florens, "Validation of a vibration and electric model of honeycomb panels equipped with piezoelectric patch actuators," *Revue des composites et des matériaux avancés*, vol. 19, no. 3, pp. 319–338, 2009.

[9] E. Balmes, M. Guskov, M. Rebillat, and N. Mechbal, "Effects of temperature on the impedance of piezoelectric actuators used for SHM," *14th Symposium on Vibration, Shock and Noise (VISHNO)*, pp. 1–6, June 2014.

[10] C.-T. Ng and M. Veidt, "A Lamb-wave-based technique for damage detection in composite laminates," *Smart materials and structures*, vol. 18, no. 7, p. 074006, 2009.

[11] V. N. Smelyanskiy, V. Hafiychuk, D. G. Luchinsky, R. Tyson, J. Miller, and C. Banks, "Modeling wave propagation in Sandwich Composite Plates for Structural Health Monitoring," in *Annual Conference of the Prognostics and Health Management Society*, pp. 1–10, 2011.

[12] B. Lamboul and D. Osmont, "Delamination detection in foam core composite structures using transient flexural wavefields," *Journal of Sound and Vibration*, vol. 366, pp. 190–198, Mar. 2016.

[13] E. Balmes and A. Deraemaeker, "Modeling structures with piezoelectric materials," *SDT tutorial*, 2013.

[14] O. M. Mukdadi, Y. M. Desai, S. K. Datta, A. H. Shah, and A. J. Niklasson, "Elastic guided waves in a layered plate with rectangular cross section," *The Journal of the Acoustical Society of America*, vol. 112, no. 5, pp. 1766–1779, 2002.

[15] D. D. Zakharov, "Orthogonality of 3d guided waves in viscoelastic laminates and far field evaluation to a local acoustic source," *International Journal of Solids and Structures*, vol. 45, pp. 1788–1803, Mar. 2008.

[16] A. Sternchüss, E. Balmes, P. Jean, and J. Lombard, "Reduction of Multistage disk models : application to an industrial rotor," *Journal of Engineering for Gas Turbines and Power*, vol. 131, 2009. Paper Number GT2008-012502.

[17] E. Balmes, *Viscoelastic vibration toolbox, User Manual*. SDTools, 2004-2013.

[18] C. Hammami, E. Balmes, and M. Guskov, "Numerical design and test on an assembled structure of a bolted joint with viscoelastic damping," *Mechanical Systems and Signal Processing*, vol. 70–71, pp. 714–724, Sept. 2015.

[19] B. Mace, R., D. Duhamel, M. Brennan, J., and L. Hinke, "Finite element prediction of wave motion in structural waveguides," *J. Acous. Soc. America*, pp. 2835–2843, 2005.

[20] M. Collet, M. Ouisse, M. Ruzzene, and M. Ichchou, "Floquet–Bloch decomposition for the computation of dispersion of two-dimensional periodic, damped mechanical systems," *International Journal of Solids and Structures*, vol. 48, pp. 2837–2848, Oct. 2011.

[21] E. Balmes, M. Rebillat, and E. Arlaud, "Wave damping and evanescence: how to combine the spatial and temporal visions of the same problem?," in *CFA, VISHNO, Le Mans*, Apr. 2016.

[22] M. Géradin and D. Rixen, *Mechanical Vibrations. Theory and Application to Structural Dynamics.* John Wiley & Wiley and Sons, 1994, also in French, Masson, Paris, 1993.